DOE/ER/60592--T2

Particle Deposition in Human and Canine Tracheobronchial Casts

DOE/ER/60592--T2

DE90 001152

IV. PROGRESS REPORT

A. Flow Distribution in Lung Airway Casts: Inhalation

To predict deposition efficiency, knowledge is required of airway morphometry and the distributions of inhaled airflow. The latter are expected to vary with flow rate and detailed measurements are needed to quantitate this parameter in the human and dog models. These data should provide essential input for the development of modifying factors to incorporate flow dependent, non-homogeneous mass transfer needed for quantitative dosimetry.

Full morphometric and inhalation flow distribution measurements on the human and canine airway casts were completed in the current grant period. The work provided new quantitative data of airflow distribution in a realistic central airway cast for two species and for two different airflow patterns; steady inspiratory flow and pulsatile inspiratory flow. The work is summarized below. Further details may be found in Appendix B. The manuscript (Appendix B) has been accepted for publication in Health Physics.

preprint removed ds

Two hollow airway casts were produced, one human and one canine (Figure A1). The humans lungs were obtained at autopsy from a 45 year

---

old male (wt. 59 kg, ht. 1.7 m), the canine lung from a mixed breed animal (approximate wt. 22 kg). The whole lungs were freeze-dried while inflated to a pressure of 2.5 kPa (25 cm H_2O). Total lung volumes after fixing were 5.2 L and 2.2 L for the human and dog respectively. The airways were cast with microcrystalline petroleum wax to the level of the terminal bronchioles. In order to completely cast all regions to this level in the canine lung, it was necessary to permit the wax to penetrate more deeply in some regions. The lung tissue was macerated from the cast using concentrated NaOH. The solid cast was then pruned back to retain airways larger than 0.5 mm.

The number of airway generations from the trachea (generation 0) to the terminal airway of the cast for each of the three complete pathways as shown in Table A1. Morphometric measurements included airway branch midpoint diameter, length, and branching angle. Measurements were made on the wax casts through the fifth generation for all branches, and to the terminal airways along three single paths of our models; a major branch path which follows the larger airway at each bifurcation, a minor branch path selecting the smaller branch at each bifurcation, and a path which alternately selects major and minor branches. All branches secondary to the three primary paths were also measured. Tables A2 and A3 summarize the morphometric data through the 10th generation for the human and canine casts respectively.

Airway branching pattern along the major pathway is very similar for the human and canine casts, with the paths terminating on the dorsal edge of the caudal side of the lower right lobe. Differences in branching pattern are more apparent in the upper lobes; however, the minor and

alternating pathways terminate near one another on both human and canine casts.

Hollow casts were produced by coating the solid wax casts with Silicone rubber (Dow Corning 3145 RTV). Many thin layers were necessary in order to preserve the distinction of the smallest airways. Thicker layers were added to the larger airways for mechanical support. Each terminal airway was trimmed open and the wax was melted out of the positive cast. Residual wax was removed by washing the cast in hot oil. There were over one thousand terminal airways on each hollow cast.

During the experiments either the human, or the canine, hollow cast was attached to a calibrated pneumotachograph (Fleisch number 1) to monitor the supply of air into the trachea. The distribution of airflow was measured at constant flow rates of 15, 30, 45 and 60 L min^{-1} for the human, and 7.5, 15, 22.5 and 30 L min^{-1} for the canine. These are equivalent to minute volumes of 6, 11, 17 and 22 L min^{-1} for the human and 3, 6, 8 and 11 L min^{-1} for the canine, assuming a breathing pattern of 3/8 inspiration, 3/8 expiration with pauses of 1/8 of a cycle after inspiration and expiration. Flow rate values used for the canine model were chosen to be one half those used in the human model because the dog lung was nearly half the size of the human. These values are consistent with a minute volume of 2.9 L min^{-1} reported for anaesthetized dogs of about the same size.

The pressure drop through the cast was less than 10 Pa (1 mm H_2O), which made it difficult to make a measurement without perturbing the flow distribution. A pressure balancing system was devised in which the

segment of the cast peripheral to the branch to be measured was sealed into a plastic bag connecting via a flow balance valve to a soap-film flow meter. The entire cast was sealed into the outer chamber which connected to a separate exhaust flow restriction valve. A horizontal tube containing a soap film was placed between the outer chamber and the inner bag containing the segment. The pressure balance between the sections was maintained by adjusting the exhaust and flow-balance valves (Figure A2).

The values of flow distribution measured with this apparatus for steady flow are remarkably precise and reproducible. The pressure balance is more difficult to control for pulsatile flow. An average balance was maintained over the course of a pulse. Test measurements showed that the sum of flows measured in the individual airways was within 3% of the tracheal flow in all cases under these conditions. This demonstrates that the average pressure balance is a reasonable method for measurements of pulsatile flow distribution.

Pulsatile flow was obtained by using a positive pressure respirator (Monaghan 170C) with a switching valve (Rudolph 1400) to simulate inspiratory flow cycles. The flow was monitored by electronically integrating (Validyne FV156) the pneumotachograph signal. The flow pulses were nearly square in shape; thus, the peak flow velocity was only about 25 percent greater than the mean. Measurements of the flow distribution under pulsatile flow were compared with that for constant inspiratory flow for equivalent mean inspiratory flow rates in the trachea. The mean inspiratory flow rate was determined from the measured integrated flow volume and duration of a pulse.

The measured flow rates in a given airway segment for different flow rates into the trachea were fitted by linear regression to an equation of the form $y = ax^b$, where, y = the flow rate in the airway segment, x = the tracheal flow rate, and a and b are fitted parameters. When 'b' is near unity, 'a' represents the fraction of the total flow which passes through the segment. The coefficient of determination (r^2) was calculated for each regression of four (or more) different flow rates.

Flow distribution is represented by the calculated values a and b of the power curve. While the same set of airways were not measured on each cast, many corresponding airway segments were measured. Representative values are shown in Table A4. Values of b greater than 1 show that as airflow increases in the trachea, a larger fraction of the flow goes to the airway segment. Values less than 1 mean that a smaller fraction of the flow goes to the segment with increasing tracheal flow rate. For b equal to 1, the fraction flowing through the airway does not change as flow rate into the trachea changes. Measured flow values can be combined for appropriate bifurcating networks to obtain parameters for particular lung segments, single lobes, or for each lung. For the complete pairs of lungs, the value of b is 0.991 for the canine and 1.006 for the human during steady inspiration. The precision of the measurements was estimated from replicate experiments. There was generally much less than 1% difference between replicates. Maximum variability was 5%.

The value of b is less than 1 for most airways in the upper lobes and greater than 1 for airways in lower lobes. For both canine and

human, this is most apparent for the upper left and lower right lobes. This indicates a redistribution of flow from the upper to the lower lobes as the flow rate increases. The difference is more striking in the canine lung where the pattern is more consistent. The pattern is similar for pulsatile flow which also further increases the deviation from linearity for a given airway. For b values less than 1, a binomial sign test finds that b is consistently lower for pulsatile flow than steady flow ($p < 0.05$) in both canine and human casts. The coefficient of variation of b for all airflows measured in each cast increased from 0.21 for steady flow to 0.24 for pulsatile flow in the canine cast, and from 0.13 to 0.16 in the human cast.

The basic model system did not include a larynx, and a separate set of measurements was carried out for the human lung cast with a model larynx added to the system to test for any effect this may have had on the flow distribution. The presence of a model larynx was found to have little influence on airflow distribution in the human cast. All measurements on a complete set of distribution pathways showed less than 5% difference from steady inspiratory flow as measured without the larynx. For most measurements the difference was less than 1%. Since the canine larynx, there would be even less difference for the canine lung.

The significant redistribution of flow to the lower lung seen here for increasing steady flows is a result of the increased inertia of the air mass which is distributed through bifurcations. Flow profiles in the central airways are complex, partly because of the geometry of the airways and the asymmetric branching pattern. Also, at typical inspiratory flow rates (a few to 120 L min^{-1}), the Reynolds numbers are such

that flow changes from turbulent to laminar and back, and turbulence produced in upper airways can be carried distally on inspiration through several branching levels before being dissipated by viscous forces. The changing flow profiles result in altered mass transfer between the air and the surface area of the airway lining, which allows hot spots of deposition of gas or aerosol particles. More air passes close to these relatively hot spots than other regions of the airway surface, which should result in enhanced mass transfer. The flow profile developed at each branch point will change with flow rate. We plan to investigate how this may contribute to the change in distribution seen in these casts.

Pulsatile inspiratory flow in our model system is more realistic than steady flow. The inertial effects seen for constant flow appear to be enhanced by pulsatile flow. For pulsatile flow the b values are consistently lower in the canine upper lobes than for constant flow. Differences are not so apparent in the pulsatile flow measurements in the human cast. This difference between the species is reasonable when the path of airflow is considered with respect to the value of b. It appears that if there are more sharp bends along the path, then the flow is impeded as shown by a reduced value of b. This effect is especially apparent in the canine upper lobes, where the airway branching pattern is most different from that of the human airways. Conversely, fewer bends along the path minimizes impedance which should allow relatively more airflow shown by a b value greater than 1. This is especially noticeable in the lower lobes.

It may be assumed that downstream conditions must be considered when examining inertial effects on flow distribution. Other

investigators have made measurements at the open ends of central airways, which does not include the influence of more peripheral airways. The casts used in this study extend to airways well beyond those airway segments in which flow was measured. Any influence of the immediate downstream flow field is thus included.

The distributions of airflow in the canine and human central airways are very similar but, this work shows that the differences must be considered when studying deposition in these airways. This is particularly evident by the more dramatic way in which the flow distribution changes with flow rate for canine as compared with human morphometry. In vivo, the inertial effect on distribution of airflow is probably damped by lung tissue compliance and the tendency of airflow to redistribute from the upper to the lower lobes at higher flow rates, may be less pronounced. Nonetheless, studies of deposition in these hollow casts of human and canine tracheobronchial airways, especially at lower flow rates, should provide realistic comparisons of mass transfer to airway surfaces.

B. Flow Distribution Through Lung Airway Casts: Exhalation

Distributuion of flow was also measured during exhalation through the casts for different total flow rates. Total pressure drops of airflow through the casts are shown Table B1 for tracheal flowrates of 30 and 60 L/min. The measured airflow resistance is substantially greater during exhalation.

The distribution of gas flow to various segments of a cast were measured as previously described. Exhalant airflow distribution was

measured with the same apparatus as for inhaled flow measurements, but with air supplied to what is labelled the exhaust and to the top of the soap-film flow meter, and exiting through the pneumotachograph. Pressure balance was accomplished in the same manner as on steady inhalant airflow.

The measured exhalant flow rates in a given cast segment, for the five different flow rates supplied to the trachea, were fitted by linear regression to an equation of the form $Y = aX^b$ as described above for inhaled flow. Parameters of the log-log regressions of flow distribution are given in Table B2 for one complete set of airways in the human cast, and in Table B3 for the canine cast. The 'b' parameter represents the curvature of the regression fit, and is a measure of the inertance of the airflow. When 'b' is greater than 1.000, it is referred to as positive inertance; a larger fraction of the flow goes to this segment as the total flow rate through the trachea increases. When 'b' is less than 1.000, negative inertance means that a smaller fraction of the total flow goes to this segment. The p values given in Tables B2 and B3 are for t-test of the residuals of the regressions for 'b' being different from 1.000.

As previously reported, inertance during inhalation was much more pronounced in the canine cast, with substantially negative inertance in the upper (cranial) regions. This is much less apparent in the human cast; however, it is significantly less than 1.000 by a t-test of the residuals of the regression of the combined data for these airways, which correspond to the upper lobes of the lungs. Consequently, both human and canine casts exhibit positive inertance in the lower (caudal)

regions of the airway casts. Inertance for a whole side of a cast, either right or left, is not significantly different from 1.000.

The magnitude of inertance during exhalation was not nearly so pronounced as during inhalation, but significant differences were seen in many individual airways. In the human cast, combined regions of the lung did not exhibit significant inertance. The canine cast did exhibit some slight, but significant inertance in the combined regions during exhalation. In many airways, the trend of inertance was opposite for inhalation and exhalation. The overall distribution of inertance is considerably different during inhalation and exhalation, which is a major reason for different distribution of airflow in each direction. An extreme example of the difference between inhalation and exhalation in airflow distribution is given in Table B4 for the canine airway cast at 30 L/min. For further details see Appendix C. } preprint removed. ds

C. Deposition Models

Deposition of particles in the lung airways occurs by sedimentation, impaction, diffusion and interception; for highly charged aerosols, electrostatic image forces may also be important. The first three mechanisms depend on the aerodynamic behavior of particles whereas interception depends merely on the geometry of particles and is negligible for spherical and other relatively compact particles. In the upper airways, in which air velocities are high, there is not sufficient time for particles to deposit by gravitational settling. The dominant deposition mechanisms are therefore diffusion for very small (D_p < 0.1 μm) particles, and impaction for large particles (D_p > 2 μm).

For laminar flow in an airway, Ingham (1975) derived an expression for the deposition of particles by diffusion (η_d) as follows:

$$\eta_d = 1-0.819e^{-14.63\Delta} -0.0976e^{-89.22\Delta} -0.0325e^{-228\Delta} -0.0509e^{-125.9\Delta^{2/3}}, \quad (1)$$

where

$$\Delta = \frac{\pi L\ t_D}{4Q}, \quad (2)$$

in which L is the airway length, Q is the flow rate through the airway, and t_D is the diffusion coefficient given by

$$t_D = \frac{KTC_F}{f} \quad (3)$$

where K is the Boltzmann constant, T is the absolute temperature, f is the drag per unit velocity, and C_F is the Cunningham slip correction factor.

reprint, Appendix A, removed, ds

Equation 1 was used by Cohen (1987, Appendix A) to predict the deposition fraction for a set of experiments in replicate human lung casts which had been trimmed to retain only airways with diameters larger than 3mm. The deposition fraction was calculated for each airway using the measured values for the length of the airway and the measured fraction of the total flow which passed through the airway. Particle sizes were ~ 0.04, 0.15 and 0.20 μm; pulsatile inspiratory flow rates averaged approximately 18 and 34 L/min. The deposition probabilities in bronchial airway generations 1-6 were greater than that predicted by a

factor of about 2. Particles were ^{99m}Tc-tagged ferric oxide size classified with an Electrostatic Classifier (ESC,TSI Model 3071). The calculation assumed that the particle and activity distributions were the same, which is to be expected for monodisperse particles. Scanning electron micrographs revealed a σ_g of about 1.3 for the 0.20 μm particles.

An analysis was undertaken to examine the impact of polydispersity on the comparison between the predicted and measured deposition probabilities. The significance of deposition by inertial impaction must also be evaluated. If a lognormal particle size distribution is assumed, impaction may be an important deposition mechanism for particles in the upper size fraction.

Inertial impaction deposition of particles at the regions near the bifurcation is found from the expression given by Chan and Yu (1981).

$$\eta_i = 0.768\ \theta\ St, \tag{4}$$

where θ is the bend angle and St is the particle Stokes number given as:

$$St = \frac{4Pd^2Q}{9\pi\mu D^3}, \tag{5}$$

in which P is the particle density, d is the particle diameter, μ is the absolute viscosity, and D is the airway diameter.

For polydisperse particles of size distribution f(d), the mass deposition fraction, DE_m, is determined from the equation

$$DE_m = \frac{\int_o^\infty \eta\, d^3\, f(d)\, d(d)}{\int_o^\infty d^3\, f(d)\, d(d)}, \tag{6}$$

where η is the deposition fraction (efficiency) of a monodisperse particles of diameter d by impaction or diffusion. Assuming a lognormal distribution of d in the form

$$f(d) = \frac{1}{\sqrt{2\pi}\, \ln \sigma_g} \exp\{-\frac{(\ln d - \ln \bar{d})^2}{2\, \ln^2 \sigma_g}\} \tag{7}$$

where $\bar{d}$ is the count median diameter and σ_g is the geometric standard deviation, equation (6) can be written as

$$DE_m = \frac{1}{\sqrt{2\pi}\, \ln \sigma_g} \int_{-\infty}^{\infty} \eta(e^y) \exp\{-\frac{[y - \ln \bar{d} + 3\, \ln^2 \sigma_g]^2}{2\, \ln^2 \sigma_g}\} dy \tag{8}$$

where

$$y = \ln(d). \tag{9}$$

Equation (8) was used to calculate the deposition fraction due to different mechanisms for the conditions of the replicate cast experiment of Cohen (1987). Results of diffusional deposition for monodisperse particles and polydisperse particles of $\sigma_g = 1.3$ are shown in Figure C1. As observed, for $\Delta < 10^{-6}$, both curves are very similar. When Δ increases, the line of $\sigma_g = 1.3$ falls below the line of $\sigma_g = 1$ and the difference increases with Δ. However, a closer inspection of the calculated values reveals that the difference does not exceed 18% for the given experimental condition.

The calculated results for particle deposition by impaction are shown in Figure C2. Deposition fraction in this figure is plotted against the Stokes number for $\delta g = 1.0$ and 1.3. Contrary to the previous calculation, polydisperse particles exhibit a higher deposition fraction than the monodisperse ones. The figure shows that for Stokes numbers less than 10^{-5}, there is a negligible deposition for both monodisperse and polydisperse particles. At $\Delta = 10^{-5}$, there is a steep increase in the deposition and the rate of increase is smaller for the monodisperse particles. Comparison of the data between this results and the results of deposition by diffusion shows that deposition by impaction is always smaller than that by diffusion by at least one order of magnitude.

The total deposition by impaction and diffusion for $\delta g = 1$ and $\delta g = 1.3$ are plotted in Figure C3, along with the experimental data of Cohen (1987). Total deposition for monodisperse particles is always higher than for polydisperse. The difference between the two increases as Δ increases and becomes significant for $\Delta > 10^{-6}$. Furthermore, the experimental deposition is higher than predicted.

The difference between the experimental data and Ingham's results could stem from different conditions, such as particle size distribution, addition of impaction and the deviation of flow in the airways from the parabolic flow profile which was assumed by Ingham to derive the results. Figure C3 clearly illustrates that polydispersity will only reduce the deposition fraction. Thus, the possibility of a particle size effect is ruled out. For the conditions of those experiments, impaction is negligible compared to diffusion. This can be seen from

Table CI in which deposition by diffusion, impaction and their sum, calculated for d = 0.2 μm and Q=600 cm^3/sec, are listed for monodisperse particles. The calculated deposition fractions are shown for every 10th airway of the replicate cast of Cohen (1987), and are ordered from smallest to largest total deposition. According to Table CI, impaction is always smaller than diffusion by at least one order of magnitude, and the difference between deposition by diffusion and total deposition is small.

The flow in the first few airway generations is turbulent because of the high air flow rate. In addition, disturbances introduced into the flow at the bifurcations alter the flow development even when the flow is not turbulent. The velocity gradient at the wall in these instances will be higher than that for fully developed laminar flow. Consequently, particle deposition on the walls is enhanced. Further down the lung, the air velocity is reduced as a result of the increase in the number of airways, and the flow distribution is generally assumed to approach a parabolic profile. Since the velocity is low, all the disturbances tend to diminish rapidly. In these airways Ingham's equation gives a good approximation of the deposition by diffusion. Therefore, particle deposition by diffusion in the lung is higher than that predicted by Ingham (1975) in the first few generations, but it approaches Ingham's results as the airway generation number increases.

Deposition of particles by diffusion in an airway is shown by Ingham (1975) to depend on a non-dimensional parameter Δ given by equation (2). In this equation, when Q decreases, Δ increases and deposition fraction increases. This implies that in the lung Δ and deposition

fraction by diffusion increase with the generation number. A logarithmic-plot of deposition fraction versus Δ is shown in Figure C4 for the experimental data and Ingham's equation. It is clear from this figure that both experimental data and Ingham's results increase with Δ. Ingham's prediction seems to underestimate the experimental values. It is also evident that, log n_d found from Ingham's equation (1), increases linearly with log Δ.

In the absence of an expression for the velocity profile in the upper airways to use in the derivation of deposition efficiency by diffusion, we attempted to formulate an expression of deposition efficiency by diffusion by curve fit of the experimental data. Since Ingham's equation predicts a linear relationship between log n_d and log Δ, we assumed an expression of the form:

$$\log(n_d) = a_o + a_1 \log\Delta \qquad (10)$$

where a_o=0.472 and a_1=0.568 are found by fitting the above expression with the experimental data of Cohen (1987). The correlation coefficient for the fit was only 0.75, owing to the scattering of the data. Equation (10) is also plotted in Figure C4. In this Figure, equation (10) falls in the middle of the data points and is higher than Ingham's equation. For small Δ, it is about twice that of Ingham, but as Δ increases the difference between the two lines decreases. For sufficiently large Δ, one expects the two lines to intersect which corresponds to a location in the respiratory system where the velocity profile becomes parabolic and deposition by diffusion can be predicted from equation (1). According to Figure C4, this point should occur around $\sim 10^{-4}$. However,

more data points particularly at higher Δ are needed to provide more accurate estimates of a_o and a_1, and to determine the value of Δ at which equations (1) and (10) yield identical results. They may permit a test of the hypothesis of a parabolic flow profile and/or that a more pronounced axial core of flow develops, as predicted by Briant (1988).

D. Deposition Experiments

Ten cast deposition experiments have been completed to date. Parameters of the experiments are shown in Table D1. The test casts were exposed in the artificial thorax as described in Appendix A and Section VB. Total activity penetrating the cast was calculated from the aerosol activity concentration as measured by placing filter collectors at the outlet of the aerosol generator. The filter samples were collected prior to connecting the artifical thorax and immediately after it was disconnected at the end of the exposure. The monodisperse aerosol flow rate is monitored by a calibrated mass flowmeter incorporated into the ESC. The aerosol output was multiplied by the duration of the exposure to determine total activity input. Activity deposited in the cast was measured with gamma ray probe detectors along the major, alternating and minor pathways as described in Section VB. Measurements were made at 69 positions for each cast.

Duplicate experiments are scheduled for the 0.05 um diameter particles in the human cast and for the 0.18 um particles in both the human and the dog cast before these data are analyzed in detail. Parameters for experiments to be scheduled in the remainder of the current grant year will be determined based on the results of these experiments. To

complete this phase of the research tests at higher flowrates are needed for both dog and human, as well as tests for particles with diameters intermediate to, and larger, than those already tested.

E. Bibliography - Eight grant related papers have been published or accepted for publication during the current grant period.

Cohen, B. S., Deposition of Ultrafine Particles in the Human Tracheobronchial Tree: A Determinant of the Dose from Radon Daughters, In: Radon and Its Decay Products: Occurrence, Properties and Health Effects, (Ed. P. Hopke), American Chemical Society, Washington, DC 20036, pp. 475-486, 1987.

Harley, N. H., and B. S. Cohen, Updating Radon Daughter Bronchial Dosimetry, In: Radon and Its Decay Products: Occurrence, Properties and Health Effects, (Ed. P. Hopke), American Chemical Society, Washington, DC 20036, pp. 419-429, 1987.

Cohen, B. S., and N. H. Harley, The Dosimetric Approach to Risk from Radon Progeny, In: Proceedings of the 40th Annual Conference on Engineering in Medicine and Biology, 29: 41, The Alliance for Engineering in Medicine and Biology, Washington, DC 20036, 1987.

Cohen, B. S., N. H. Harley, R. B. Schlesinger, and M. Lippmann, Nonuniform Particle Deposition on Tracheobronchial Airways: Implications for Lung Dosimetry, Ann. Occup. Hyg. 32: 1045-1053, Supplement 1, 1988.

Cohen, B. S., Sampling Airborne Radioactivity, In: Air Sampling Instruments, 7th Edition, (Eds. S. Hering and P. Lioy), Am. Conf. Govt. Ind.

Hygienists, Cincinnati, OH 45211-4438 (In press).

Cohen, B. S., and J. K. Briant, Flow Distributuion in Lung Airway Casts of Human and Canine Tracheobronchial Trees, Health Phys. (In press).

Cohen, B. S., R. G. Sussman, and M. Lippmann, Ultrafine Particle Deposition in a Human Tracheobronchial Cast, Aerosol Science and Technology (in press).

Briant, J. K., and B. S. Cohen, Flow Distribution Through Human and Canine Airways During Inhalation and Exhalation, Journal of Applied Physiology, (in press).

List of Tables

Table C1. Deposition efficiency of particles by diffusion, impaction, and sum of the two, in selected airways of the replicate cast for d=0.2 μm and Q=600 cm^3/sec.

Table D1. Parameters of the cast deposition experiments.

Table A1. Number of airway generations per path through the human and canine airway models (diameter of smallest airway, mm)

	Minor	Alternate	Major
Human	8 (0.7)	10 (0.8)	29 (0.4)
Canine	7 (0.5)	8 (0.5)	28 (0.6)

Table A2. Morphometry of the human cast for the first 10 generations. Length and diameter for the Weibel Model A (Weibel 1963) are shown for comparison. All airways are included for generations 0 to 5 (see text)

Generation	Number of Airways	Length (mm)	Diameter (mm)	Flow Angle (degrees)	Weibel Model A	
					Length (mm)	Diameter (mm)
0	1	100.0	18.6	0	120	18.0
1	2	43.3 (0.43)*	13.2 (0.11)	38.5 (0.13)	47.6	12.2
2	4	15.9 (0.44)	8.6 (0.16)	38.8 (0.68)	19.0	8.3
3	8	11.6 (0.63)	6.6 (0.13)	38.2 (0.67)	7.6	5.6
4	16	12.1 (0.38)	5.4 (0.22)	34.6 (0.87)	12.7	4.5
5	32	11.0 (0.47)	4.9 (0.26)	31.6 (0.81)	10.7	3.5
6	6	11.3 (0.20)	3.5 (0.44)	22.2 (0.95)	9.0	2.8
7	6	8.0 (0.38)	3.1 (0.72)	39.5 (0.76)	7.6	2.3
8	6	8.8 (0.90)	2.5 (0.80)	28.7 (1.0)	6.4	1.9
9	4	5.2 (0.68)	2.8 (0.51)	32.0 (1.3)	5.4	1.5

*Mean (coefficient of variation)

Table A3. Morphometry of the Canine Cast for the first 10 generations. All airways are included for generations 0 to 5 (see text)

Generation	Number of Airways	Length (mm)	Diameter (mm)	Flow Angle (degrees)
0	1	227.5	20.3	0
1	2	20.6 (0.10)[a]	18.4 (0.11)	26.0 (0.49)
2	4	15.3 (0.37)	11.8 (0.36)	30.0 (1.3)
3	8	9.5 (0.62)	9.1 (0.44)	38.8 (0.75)
4	16	9.7 (0.50)	6.6 (0.47)	23.1 (0.95)
5	32	6.0 (0.47)	4.6 (0.58)	30.2 (1.1)
6	6	6.1 (1.1)	4.1 (0.94)	43.3 (0.66)
7	6	1.3 (1.3)	4.0 (1.2)	18.0 (2.2)
8	6	8.2 (0.93)	3.5 (0.84)	27.5 (0.13)
9	2	3.1 (1.4)	7.4 (0.30)	15.0 (1.4)

[a]Mean (coefficient of variation)

Table A4a. Flow distributions for both steady inspiratory (a) and pulsatile (b) flow are listed as parameters of a linear regression to the equation $y = ax^b$

Airway		Canine			Human		
		a	b	r^2	a	b	r^2
Upper							
Left	12222	0.0072	0.928	0.988	0.0392	0.710	1.000
	1222	0.0683	0.726	0.999	0.1171	0.899	1.000
	12212	0.0398	0.664	0.993	0.0371	1.101	0.999
	12211	0.1060	0.706	0.992	0.0468	1.058	1.000
	1212	0.0934	0.863	0.996	0.1077	0.805	0.999
Right	1122	0.0529	0.810	0.997	0.0666	0.980	1.000
	1121	0.1758	0.766	0.998	0.1294	1.019	1.000
Lower							
Left	12112	0.0650	1.132	0.998	0.0472	1.062	0.999
	12111	0.1589	1.066	0.999	0.1237	0.062	1.000
Right	1112	0.0641	1.094	0.999	0.0715	1.059	1.000
	11112	0.0495	1.184	0.999	0.0783	0.899	0.999
	111112	0.0405	0.962	1.000	0.0598	0.925	1.000
	1111112	0.0542	1.147	0.999	0.0493	0.960	0.999
	111111	0.2808	1.035	0.995	0.1558	1.014	0.999
	1111111	0.2285	0.998	0.993	0.0906	1.083	1.000
Left Lung		0.4344	0.974	1.000	0.4591	1.002	1.000
Right Lung		0.6338	1.002	0.999	0.5365	1.009	1.000
Total Lungs		1.0680	0.991	1.000	0.9955	1.006	1.000

Table A4b. Flow distributions for both steady inspiratory (a) and pulsatile (b) flow are listed as parameters of a linear regression to the equation $y = ax^b$

Airway		Canine			Human		
		a	b	r^2	a	b	r^2
Upper							
Left	12222	0.0131	0.696	0.933			
	1222	0.0833	0.647	0.996	0.1222	0.860	1.000
	12212	0.0470	0.588	0.994	0.0392	1.059	0.999
	12211	0.1310	0.612	1.000	0.0397	1.073	1.000
	1212	0.0434	0.744	0.993	0.1179	0.758	0.999
Right	1122	0.0544	0.766	0.995	0.0706	0.945	1.000
	1121	0.2221	0.656	0.995	0.1323	0.989	1.000
Lower							
Left	12112	0.0626	1.116	0.998	0.0360	1.103	0.998
	12111	0.1741	1.005	0.999	0.1337	1.018	0.999
Right	1112	0.0598	1.087	1.000	0.0790	1.007	1.000
	11112	0.0473	1.167	0.999	0.0914	0.836	0.998
	111112	0.0461	0.885	0.997	0.0571	0.920	1.000
	1111112	0.0510	1.132	0.997	0.0507	0.932	0.999
	111111	0.2323	1.072	0.999			
	1111111	0.1821	1.051	0.999	0.0898	1.062	1.000
Left Lung		0.4717	0.919	1.000	0.4521	0.978	1.000
Right Lung		0.5925	0.995	1.000	0.5570	0.976	1.000
Total Lungs		1.0596	0.965	1.000	1.0090	0.977	1.000

Table B1. Total pressure drops of airflow through the hollow airway casts are given in mm H_2O.

	Total Flow Rate	
	30 L/min	60 L/min
Human		
Inhalation	0.5	1.3
Exhalation	1.0	3.0
Canine		
Inhalation	0.1	0.2
Exhalation	0.6	1.9

Table B2. Distribution of inhalant and exhalant airflow in the human airway cast is listed as the parameters of a linear regression to the equation $Y=aX^b$.

			Inhalation			Exhalation		
		AIRWAY	a	b	r^2	a	b	r^2
Upper	Left	1222	0.1171	0.899*	1.000	0.1111	0.987*	1.000
		12212	0.0371	1.101*	0.999	0.0460	1.005*	1.000
		12211	0.0468	1.058*	1.000	0.0516	1.005*	1.000
		1212	0.1077	0.805*	0.999	0.0883	1.004*	1.000
	Right	1122	0.0666	0.980*	1.000	0.0808	1.023*	1.000
		11212	0.0545	1.016*	1.000	0.0617	1.055*	0.999
		11211	0.0749	1.020*	1.000	0.0889	0.980*	1.000
Lower	Left	12112	0.0472	1.062*	0.999	0.0483	1.023*	1.000
		12111	0.1237	1.062*	1.000	0.1279	0.983*	1.000
	Right	1112	0.0715	1.059*	1.000	0.0858	1.020*	1.000
		11112	0.0783	0.899*	0.999	0.0728	0.986*	0.999
		111112	0.0598	0.925*	1.000	0.0555	0.978*	1.000
		1111112	0.0493	0.960*	0.999	0.0468	0.935*	1.000
		1111111	0.0906	1.083*	1.000	0.0827	0.973*	1.000
		Upper Lobes	0.4861	0.977*	1.000	0.5273	1.007o	1.000
		Lower Lobes	0.5122	1.029+	1.000	0.5184	0.989o	1.000
		Left Lung	0.4591	1.002o	1.000	0.4728	0.997o	1.000
		Right Lung	0.5365	1.009o	1.000	0.5726	0.999o	1.000
		Total Lungs	0.9955	1.006o	1.000	1.0455	0.998o	1.000

*** P < 0.001**
+ 0.001 < P < 0.01
o P > 0.01

Table B3. Distribution of inhalant and exhalant airflow in the canine airway cast is listed as the parameters of a linear regression to the equation $Y=aX^b$.

		AIRWAY	Inhalation a	Inhalation b	Inhalation r^2	Exhalation a	Exhalation b	Exhalation r^2
Upper	Left	1222	0.0683	0.726*	0.999	0.0613	0.968*	1.000
		12212	0.0398	0.664*	0.993	0.0273	1.011*	0.999
		12211	0.1060	0.706*	0.992	0.0671	1.054*	1.000
		1212	0.0334	0.863*	0.997	0.0316	1.020*	1.000
	Right	1122	0.0529	0.810*	0.997	0.0547	0.970*	0.999
		11212	0.0403	0.757*	0.998	0.0343	1.004*	0.999
		11211	0.1356	0.769*	0.997	0.0974	1.040*	1.000
Lower	Left	12112	0.0650	1.132*	0.998	0.0851	1.003*	1.000
		12111	0.1589	1.066*	0.999	0.1884	0.973*	1.000
	Right	1112	0.0641	1.094*	0.999	0.0853	0.986*	1.000
		11112	0.0495	1.184*	0.999	0.0642	1.002o	1.000
		111112	0.0405	0.962*	1.000	0.0358	1.030*	0.999
		1111112	0.0542	1.147*	0.999	0.0633	0.969*	0.998
		1111111	0.2285	0.998o	0.993	0.1388	1.066*	0.998
		Upper Lobes	0.4730	0.757*	0.998	0.3728	1.016*	1.000
		Lower Lobes	0.6551	1.070*	0.999	0.6597	1.006+	1.000
		Left Lung	0.4344	0.974*	1.000	0.4596	0.997o	1.000
		Right Lung	0.6338	1.002o	0.999	0.5731	1.019*	1.000
		Total Lungs	1.0680	0.991o	1.000	1.0324	1.010+	1.000

* $P < 0.001$
\+ $0.001 < P < 0.01$
o $P > 0.01$

Table B4. Distribution of inhalant and exhalant airflow in the canine airway cast is listed as the volume flow rate measured during a steady flow of 30 L/min in the trachea (all values L/min).

		AIRWAY	Inhalation	Exhalation
Upper	Left	1222	0.80	1.64
		12212	0.36	0.84
		12211	1.13	2.41
		1212	0.64	1.01
	Right	1122	0.84	1.48
		11212	0.51	1.06
		11211	1.85	3.31
Lower	Left	12112	3.19	2.58
		12111	5.77	5.13
	Right	1112	2.68	2.46
		11112	2.77	1.97
		111112	1.05	1.17
		1111112	2.63	1.75
		1111111	6.90	5.08
		Upper Lobes	6.13	11.76
		Lower Lobes	24.99	20.15
		Left Lung	11.89	13.60
		Right Lung	19.24	18.31
		Total Lungs	31.13	31.91

Table C1. Deposition efficiency of particles by diffusion, impaction, and sum of the two, in selected airways of the replicate cast for d=0.2 μm and Q=600 cm^3/sec.

L (cm)	D (cm)	η_d	η_i	$\eta_d+\eta_i$
1.06	0.75	4.91×10^{-5}	4.3×10^{-6}	5.34×10^{-5}
0.71	0.57	5.11×10^{-5}	5.43×10^{-6}	5.66×10^{-5}
9	1.9	5.58×10^{-5}	6.22×10^{-6}	6.20×10^{-5}
0.85	0.39	1.34×10^{-4}	8.47×10^{-6}	1.42×10^{-4}
0.97	0.41	1.35×10^{-4}	8.93×10^{-6}	1.44×10^{-4}
1.03	0.37	1.33×10^{-4}	1.54×10^{-5}	1.48×10^{-4}
2.46	0.55	1.57×10^{-4}	1.41×10^{-5}	1.71×10^{-4}
0.81	0.36	1.67×10^{-4}	7.64×10^{-6}	1.75×10^{-4}
1	0.33	1.78×10^{-4}	1.50×10^{-5}	1.93×10^{-4}
0.64	0.29	1.92×10^{-4}	9.21×10^{-6}	2.01×10^{-4}
2.25	0.44	1.84×10^{-4}	2.29×10^{-5}	2.07×10^{-4}
1.04	0.34	1.97×10^{-4}	1.23×10^{-5}	2.09×10^{-4}
0.62	0.32	2.07×10^{-4}	5.22×10^{-6}	2.12×10^{-4}
0.75	0.25	2.74×10^{-4}	1.35×10^{-5}	2.88×10^{-4}

Table D1. Parameters of the cast deposition experiments

Cast	Particle Size d (μm)	Average Inspiratory Flow Rate L/M	Breaths Per Minute
Canine	0.05	13.1	25
Canine	0.05	11.5	18
Canine	0.10	14.6	33
Canine	0.10	11.1	28
Canine	0.10	13.8	36
Canine	0.18	19.2	22
Human	0.05	11.2	14
Human	0.10	18.0	15
Human	0.10	13.3	18
Human	0.18	20.6	20

List of Figures

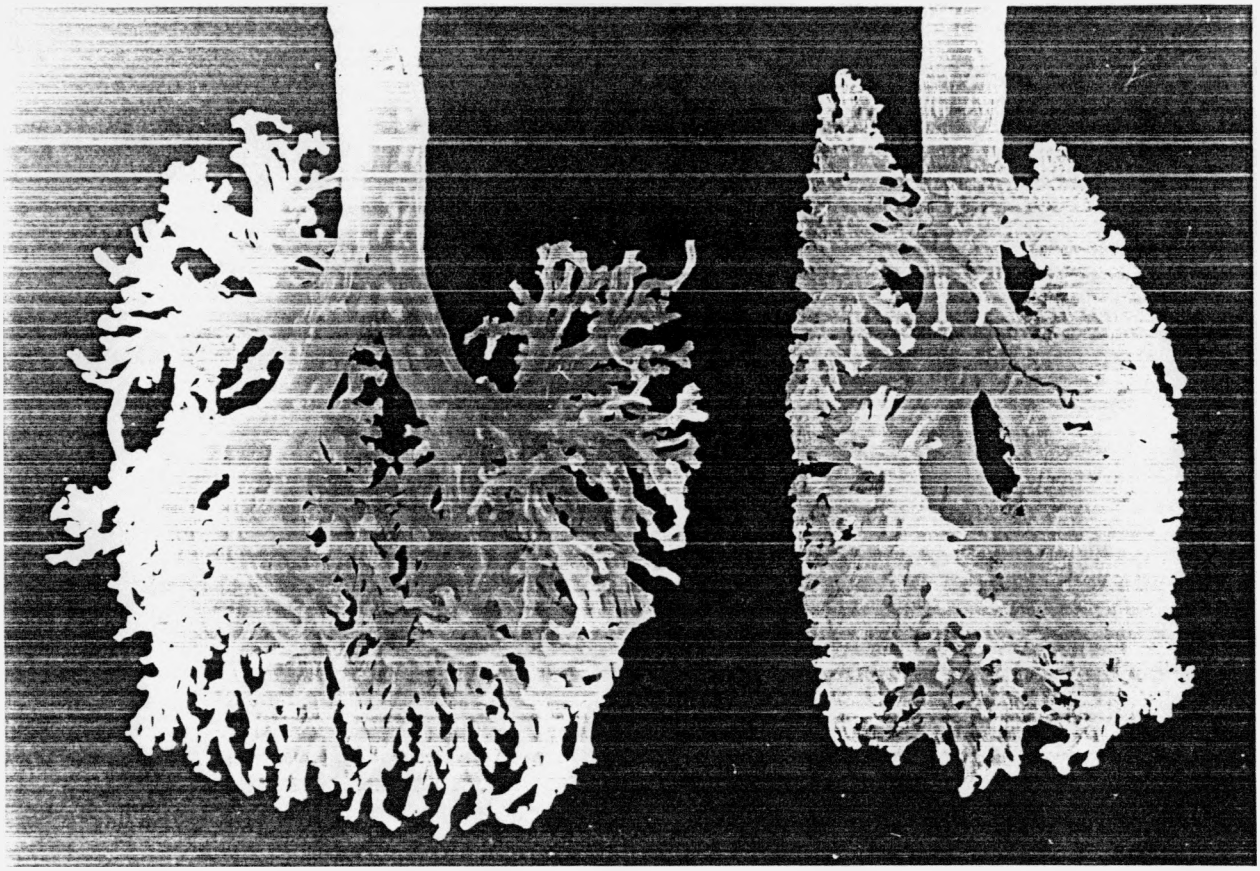

Figure A1. Hollow silicone rubber casts of human (left) and canine (right) central airways. Terminal airways are < 1 mm in diameter.

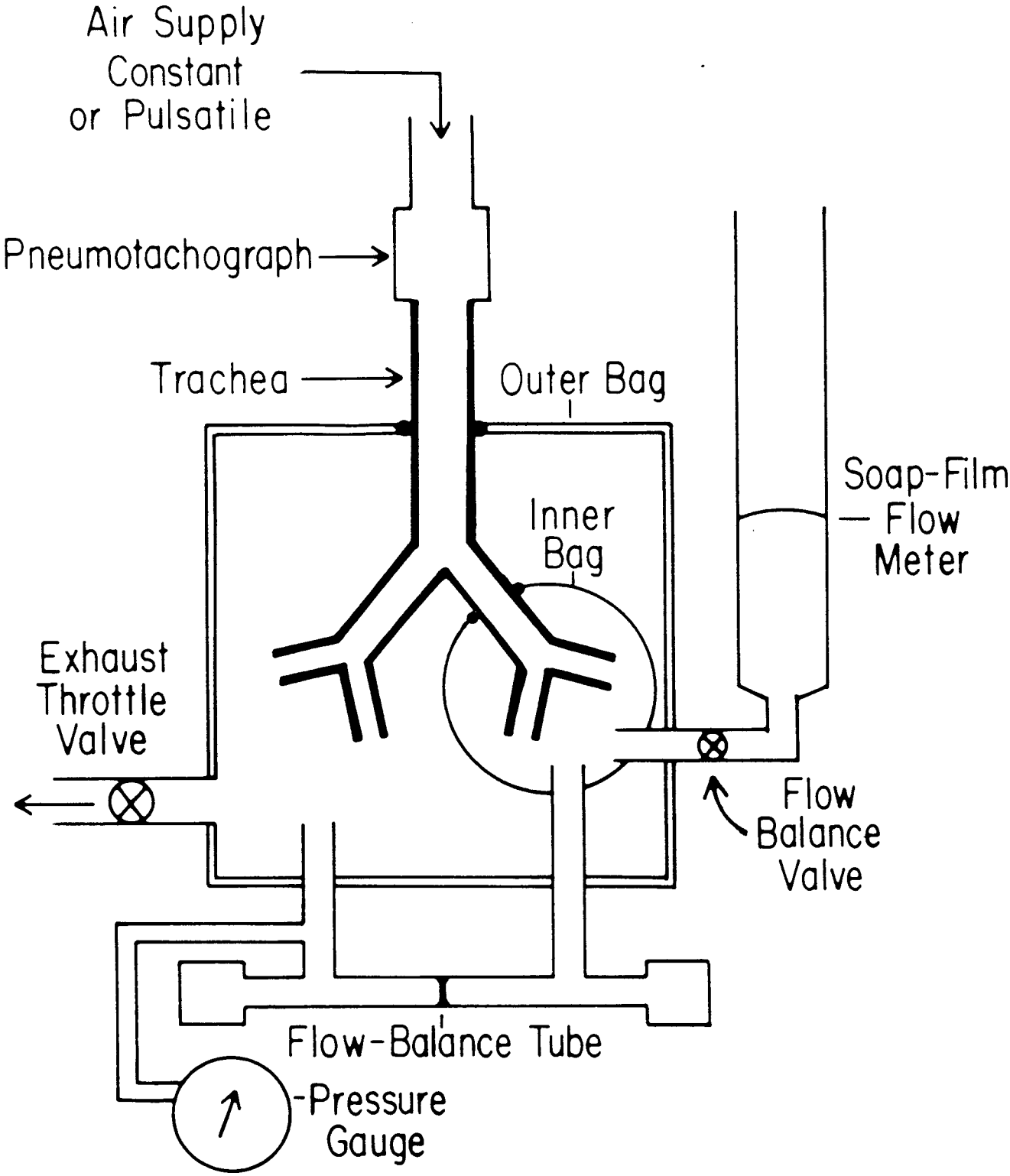

Airflow Distribution Measurement
in a Hollow Airway Cast

Figure A2

Figure A3

DIVISION OF AIRFLOW BY AERODYNAMIC IMPEDANCE OF STEADY FLOW IN TRACHEOBRONCHIAL TREE CASTS
(values in percent of tracheal volume flow rate)

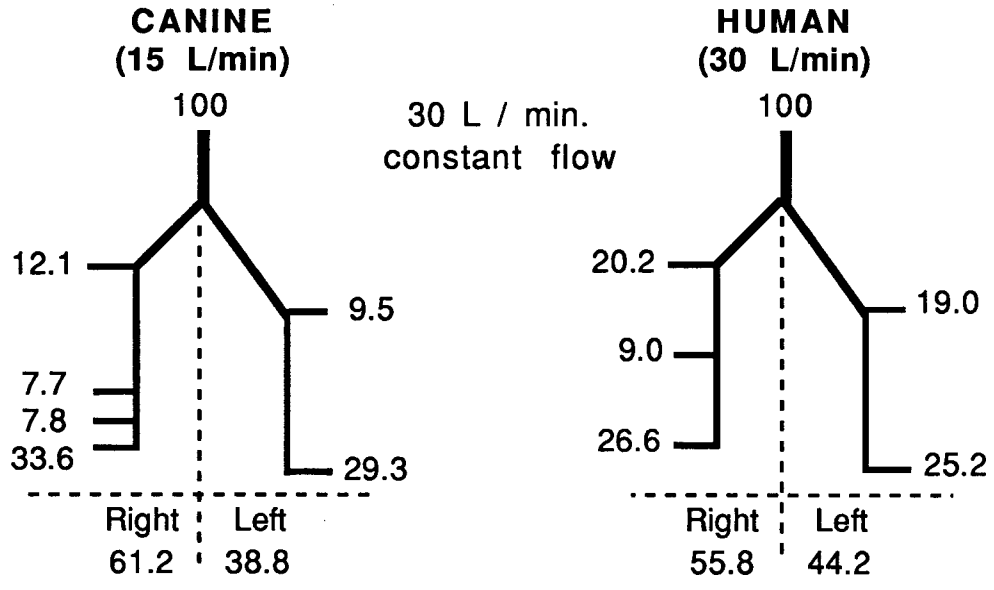

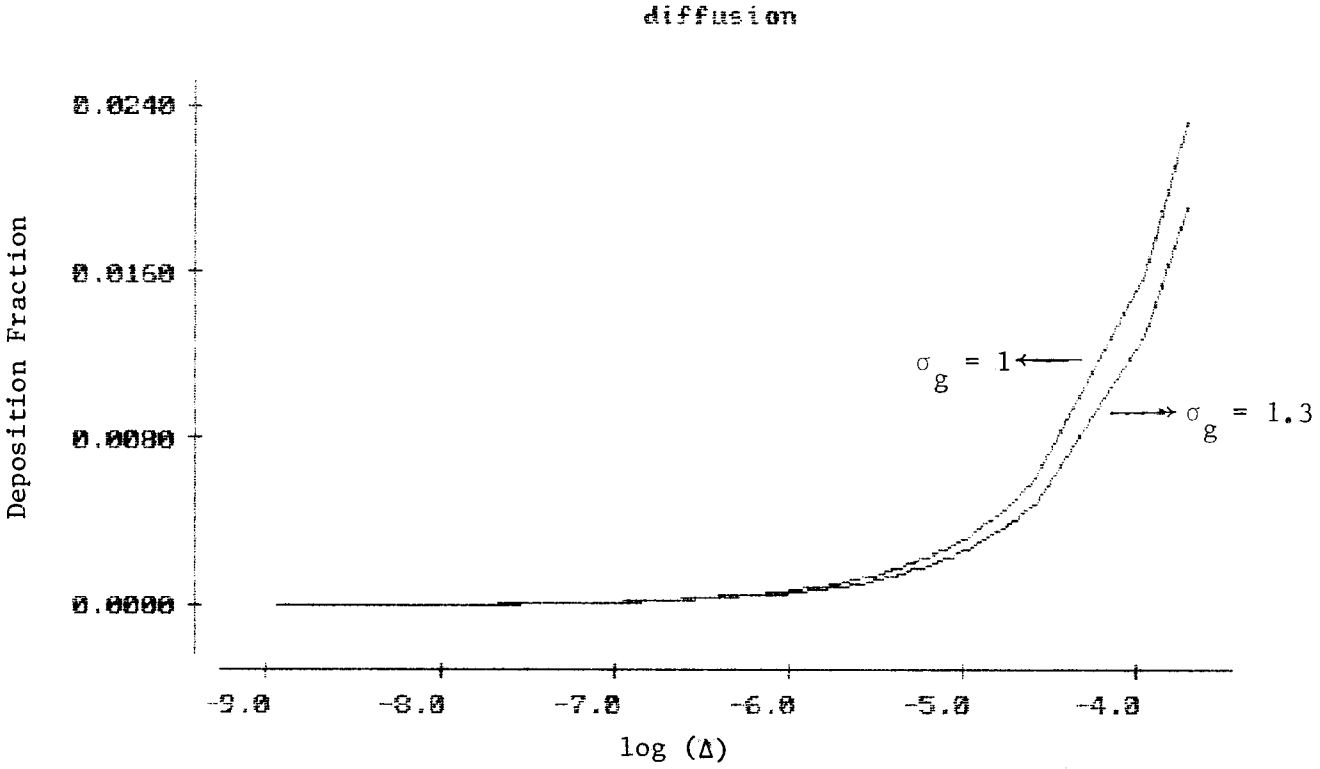

Fig. C1

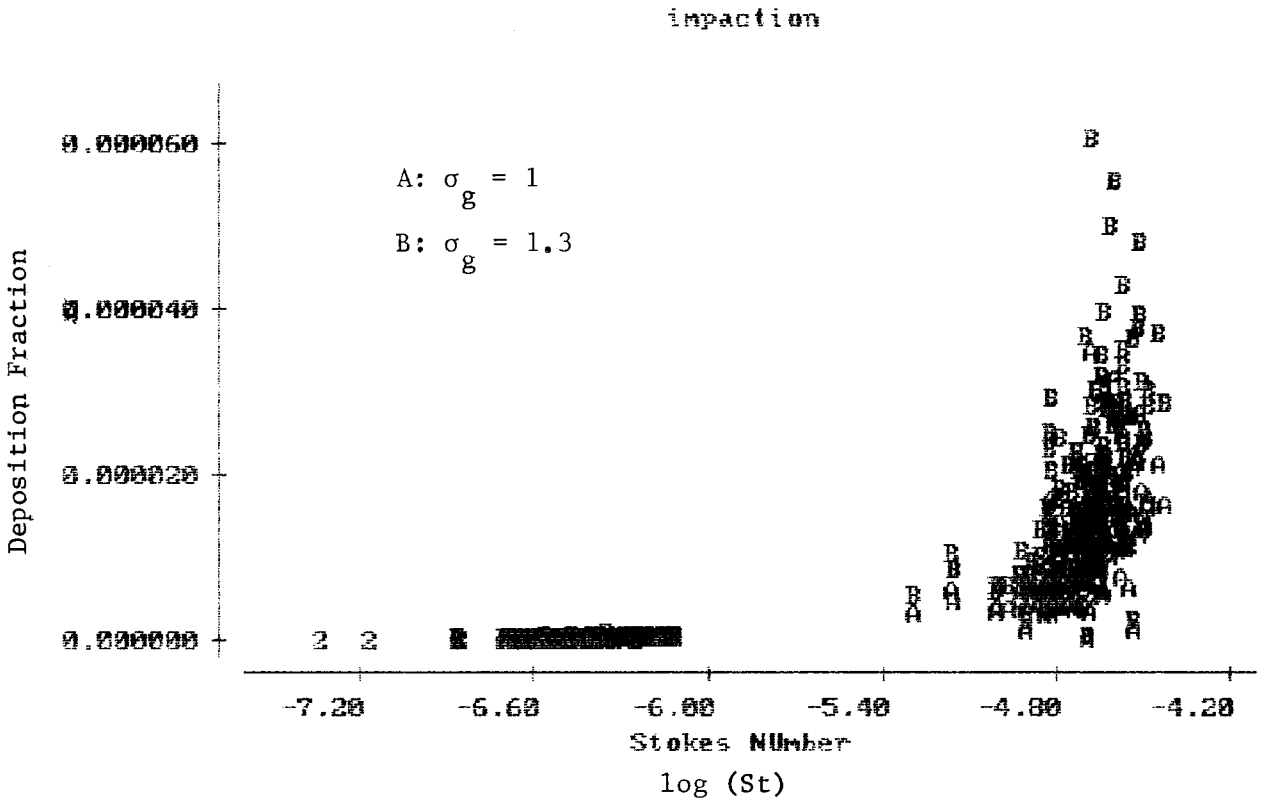

Fig. C2

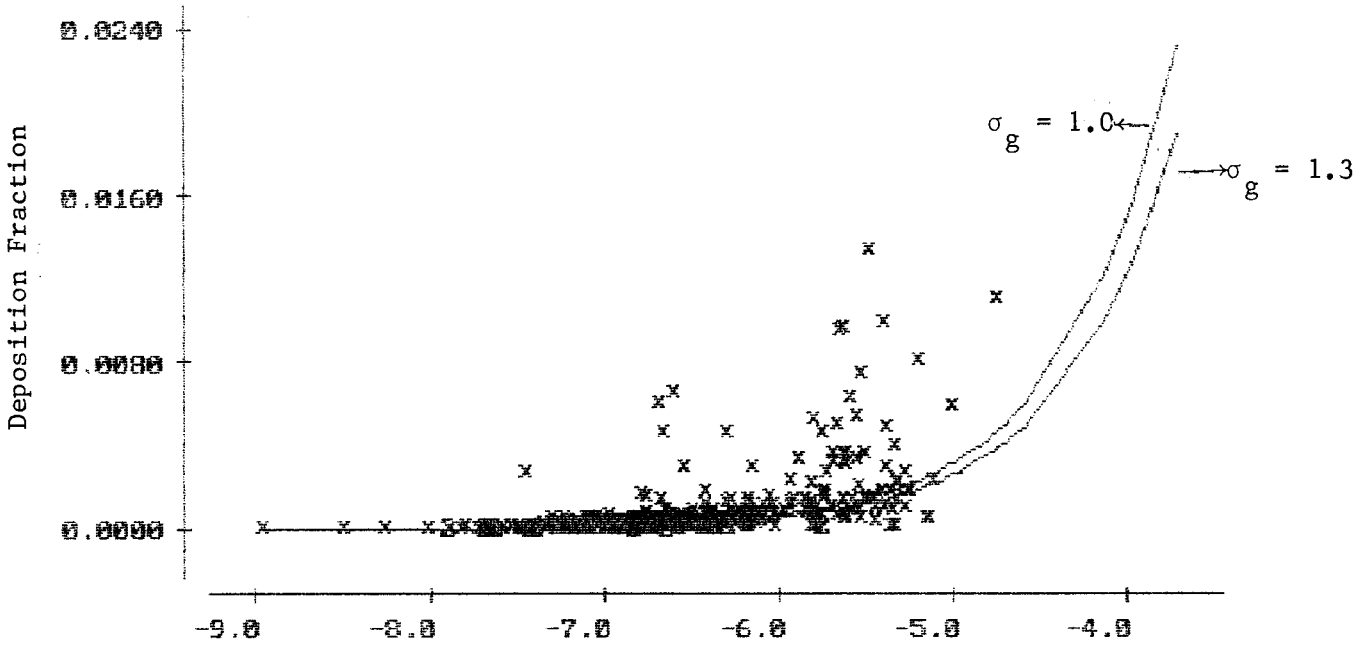

Fig. C3

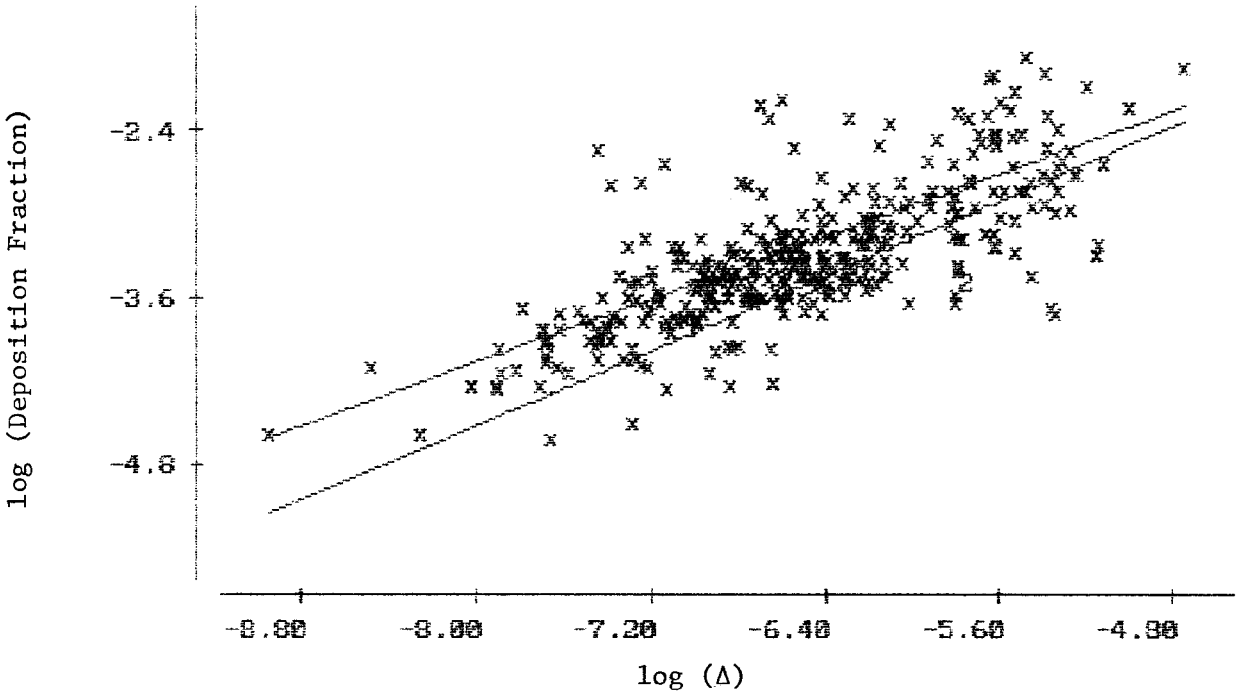

Fig. C4

preprints removed.